Electronic Supplementary Material

Novel hierarchical yolk-shell α-$Ni(OH)_2/Mn_2O_3$ microspheres as high specific capacitance electrode materials for supercapacitors

Xiqing Luo*, Miaomiao Jiang*, Kun Shi (✉), Zhangxian Chen, Zeheng Yang (✉), Weixin Zhang (✉)

School of Chemistry and Chemical Engineering, Hefei University of Technology and Anhui Key Laboratory of Controllable Chemical Reaction & Material Chemical Engineering, Hefei 230009, China

E-mails: shikun@hfut.edu.cn (Shi K); zehengyang@hfut.edu.cn (Yang Z); wxzhang@hfut.edu.cn (Zhang W).

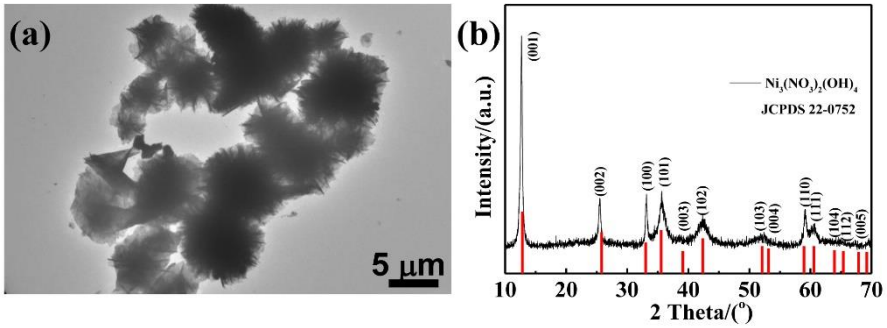

Fig. S1 (a) SEM image and (b) XRD pattern of the $Ni_3(NO_3)_2(OH)_4$ product.

In order to verify the role of oleylamine in the preparation of yolk-shell α-$Ni(OH)_2/Mn_2O_3$ microspheres, controlled experiment has been conducted by the same synthesized method of yolk-shell α-$Ni(OH)_2$ microspheres, but without the addition of oleylamine. As shown in Fig. S1a, the products prepared here exhibit irregular morphology rather than yolk-shell structure, mainly due to the absence of oleylamine as surfactants to stabilize the produced bubble-assisted soft templates in the boiling reaction solution [1]. Furthermore, the XRD pattern display the composition of the product as $Ni_3(NO_3)_2(OH)_4$ instead of α-$Ni(OH)_2$ (Fig. S1b), which can demonstrates from the reverse side that oleylamine also plays a key role of precipitant for the reaction to form the yolk-shell α-$Ni(OH)_2$ microspheres [2].

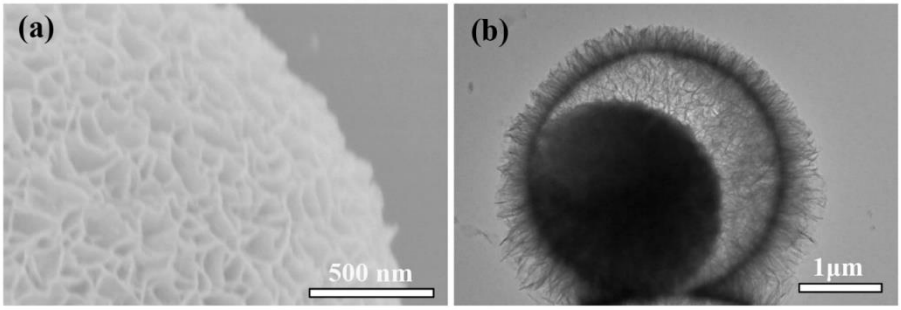

Fig. S2 (a) Enlarged SEM and (b) TEM view of the single α-$Ni(OH)_2/Mn_2O_3$ microsphere.

In the enlarged SEM image of the α-$Ni(OH)_2/Mn_2O_3$ microsphere (Fig. S2a), it can be seen that the shell of the microsphere shows porous microstructures decorated by plentiful and interconnected nanosheets. Though treated with $KMnO_4$ solution, the α-$Ni(OH)_2/Mn_2O_3$ microsphere still retain their yolk-shell microstructures, except for the relatively denser nanosheets due to the Mn_2O_3 deposition (Fig. S2b), implying the formation of hierarchical α-$Ni(OH)_2/Mn_2O_3$ hetero-structured microspheres.

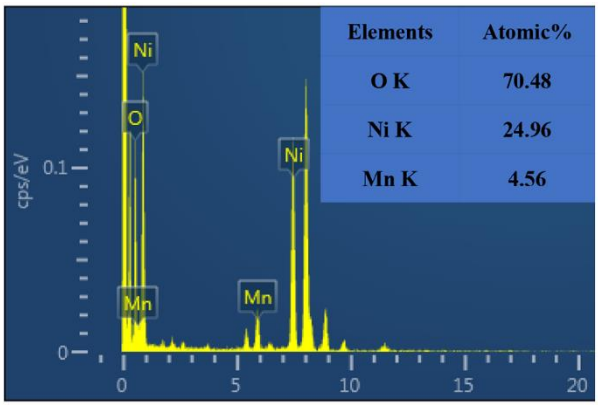

Fig. S3 Energy dispersive X-ray image of the α-$Ni(OH)_2/Mn_2O_3$ samples.

The electron mapping of the α-$Ni(OH)_2/Mn_2O_3$ microspheres are determined by EDS (Fig. S3). The atomic percentages of Ni, Mn and O are 24.96%, 4.56% and 70.48%, respectively. According to this, the mass ratio of $Ni(OH)_2$ and Mn_2O_3 can be calculated to be about 10:1.

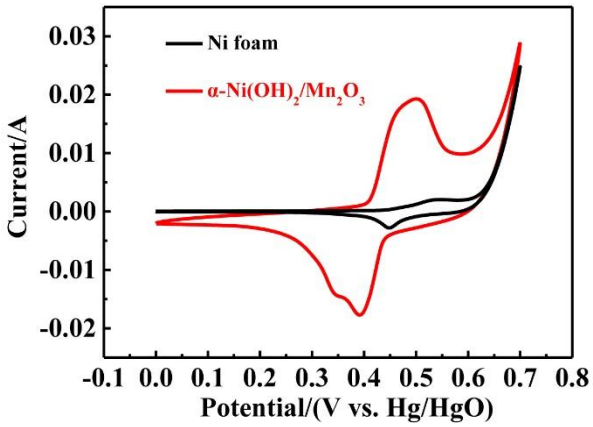

Fig. S4 CV curves of α-$Ni(OH)_2/Mn_2O_3$ and blank Ni foam at the scanning rate of 20 mV s^{-1}.

The CV test of the blank Ni foam has been performed at the scanning rate of 20 mV s^{-1} in the voltage window range from 0.0 V to 0.7 V (vs. Hg/HgO) (Fig. S4). It could be found that from the comparison between CV performance of blank Ni foam and α-$Ni(OH)_2$/Mn_2O_3, the capacitance contribution of the Ni foam substrates to the whole electrode is really very small and could be negligible.

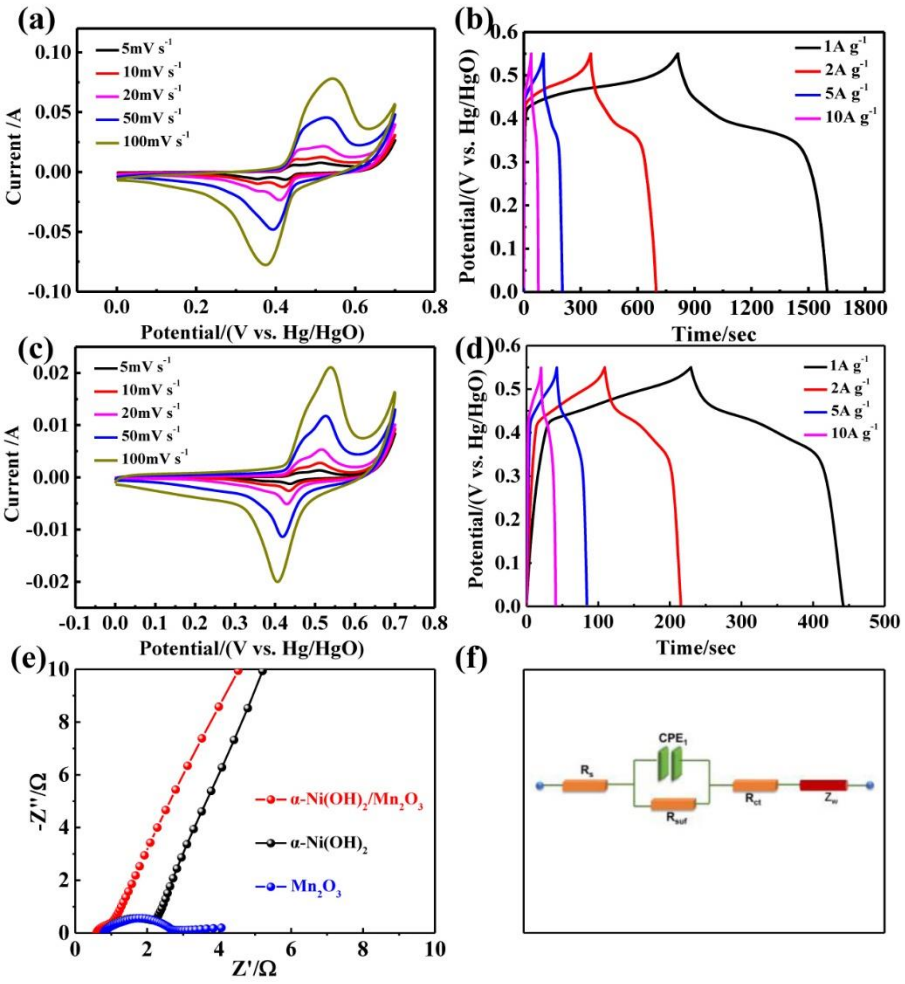

Fig. S5 Capacitance performance of the as-synthesized microspheres in 1 M KOH: (a) CV curves of α-$Ni(OH)_2$ samples at various scanning rates. (b) Galvanostatic charge-discharge curves of α-$Ni(OH)_2$ samples at different current densities, (c) CV curves of Mn_2O_3 at various scan rates, (d) GCD curves of Mn_2O_3 at different current densities, (e) EIS curves of Mn_2O_3, α-$Ni(OH)_2$ and α-$Ni(OH)_2$/ Mn_2O_3 samples, and (f) the corresponding equivalent circuit diagram.

Table S1 The fitting results of Nyquist plots.

Samples	R_s(Ω)	R_{suf}(Ω)	R_{ct}(Ω)	CPE_1(F)	CPE_2(F)	W-p
α-$Ni(OH)_2$/Mn_2O_3	0.541	0.298	0.083	1.036	0.0002	0.396
α-$Ni(OH)_2$	0.057	1.253	0.79	0.86	0.0002	0.414
Mn_2O_3	0.783	1.983	/	0.66	0.019	/

As shown in Fig. S5, the single α-$Ni(OH)_2$ microspheres and Mn_2O_3 (Shanghai Aladdin Biochemical Technology Co., Ltd) all display the representative pseudocapacitive behavior (Fig. S5a, S5c) and stable charge/discharge platforms at different current densities (Fig. S5b, S5d), but exhibit relatively low specific capacitance. Specifically, the calculated specific capacitance of α-$Ni(OH)_2$ microspheres and Mn_2O_3

samples is only 1431 F g^{-1} and 389 F g^{-1} at 1 A g^{-1} respectively, and much lower than 2228.6 F g^{-1} at 1 A g^{-1} of the yolk-shell α-$Ni(OH)_2/Mn_2O_3$ microspheres.

EIS tests have been performed to further investigate the electrochemical behaviors, the obtained Nyquist plots are displayed in Fig. S5e. According to the corresponding equivalent circuit diagram (Fig. S5f) and fitting results (Table S1), the yolk-shell α-$Ni(OH)_2/Mn_2O_3$ microspheres exhibit remarkably decreased R_{suf} resistances (0.298 Ω) in interfacial layer and R_{ct} resistances (0.083 Ω) in charge transfer processes when compared with single α-$Ni(OH)_2$ microspheres (R_{suf} = 1.253 Ω, R_{ct} = 0.79 Ω) or Mn_2O_3 (R_{suf} = 1.983 Ω), illustrating the enhanced conductivity and facilitated interface charge transfer in α-$Ni(OH)_2/Mn_2O_3$ microspheres.

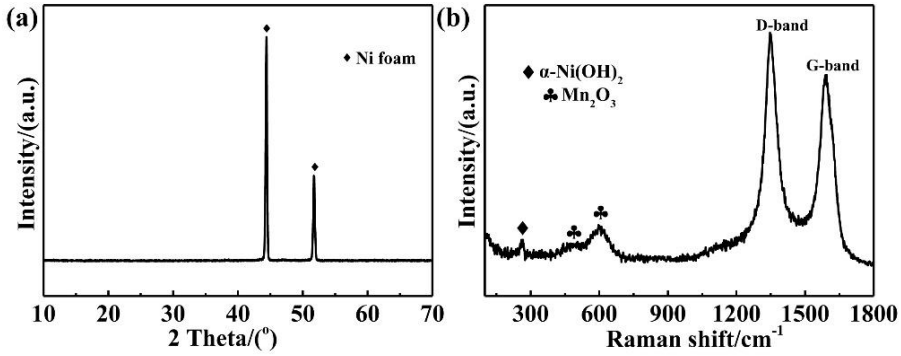

Fig. S6 (a) XRD pattern and (b) Raman spectra of α-$Ni(OH)_2/Mn_2O_3$ working electrode after 3000 cycles.

The crystal phases of α-$Ni(OH)_2/Mn_2O_3$ electrode after 3000 cycles are identified by XRD. As shown in Fig. S6a, there are no other obvious diffraction peaks except for those of Ni foam can be found, probably due to the relatively weak XRD characteristic peaks of α-$Ni(OH)_2/Mn_2O_3$ have been completely overlapped by the strong peaks of nickel foam substrate.

In order to further demonstrate the composition information of α-$Ni(OH)_2/Mn_2O_3$ electrode after 3000 cycles, Raman measurements have been performed. As shown in Fig. S6b, a new peak at 264 cm^{-1} appears relative to the α-$Ni(OH)_2/Mn_2O_3$ microspheres before cycling (Fig. 2b), which could be assigned to the vibration of Ni-OH lattice. This result may be attributed to the Ni-OH site exposure caused by long-term electrochemical cycling. Besides, the obvious peak at 600 cm^{-1} and a relatively weak peak at 480 cm^{-1} are attributed to the bending modes of Mn_2O_3, which are consistent with the composition information of α-$Ni(OH)_2/Mn_2O_3$ electrode before cycling (Fig. 2b). The D- and G-bands mainly result from the conductive acetylene black contained in the composite working electrode. Overall, the above results clearly demonstrate the excellent chemical stability of α-$Ni(OH)_2/Mn_2O_3$ electrode, even under long-term electrochemical cycling.

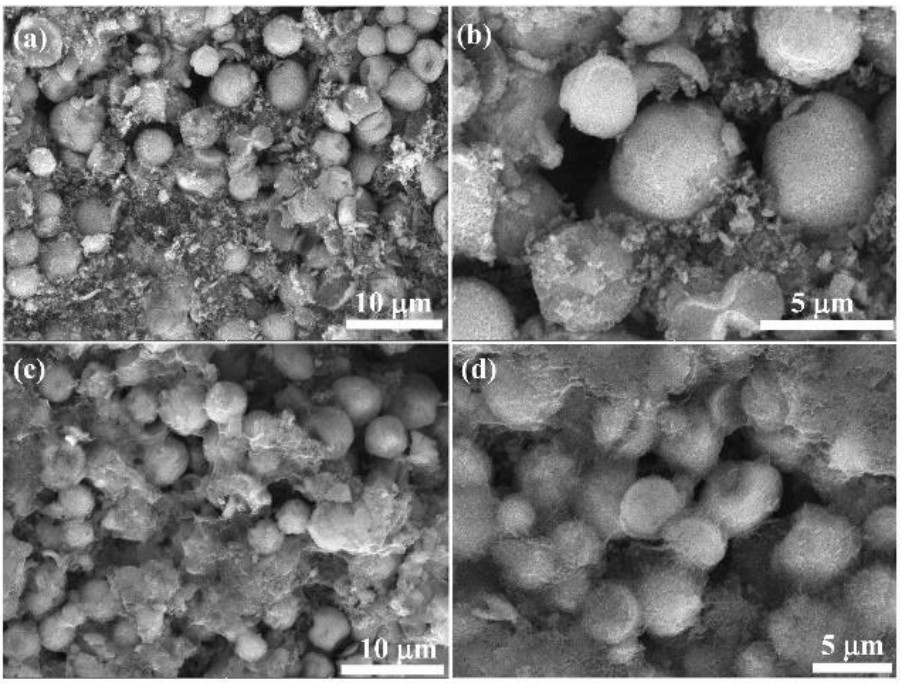

Fig. S7 Low- and high- magnification FESEM images of α-$Ni(OH)_2/Mn_2O_3$ before cycling (a, b) and after 3000 cycles (c, d).

The morphologies of the α-$Ni(OH)_2/Mn_2O_3$ electrode before and after 3000 cycles have been observed by FESEM (Fig. S7). Similar to the α-$Ni(OH)_2/Mn_2O_3$ microspheres before cycling (Fig. S7a, b), the α-$Ni(OH)_2/Mn_2O_3$ microspheres after 3000 cycles (Fig. S7c, d) show not only the almost intact physical adhesion structure, but also undamaged spherical morphology of the α-$Ni(OH)_2/Mn_2O_3$ microspheres, displaying good electrochemical stability of the α-$Ni(OH)_2/Mn_2O_3$ electrode. Which may be due to that, the out-shell Mn_2O_3 sediment distributed over the hybrid microspheres can act as an effective protective layer in the process of electrode electrochemical reaction.

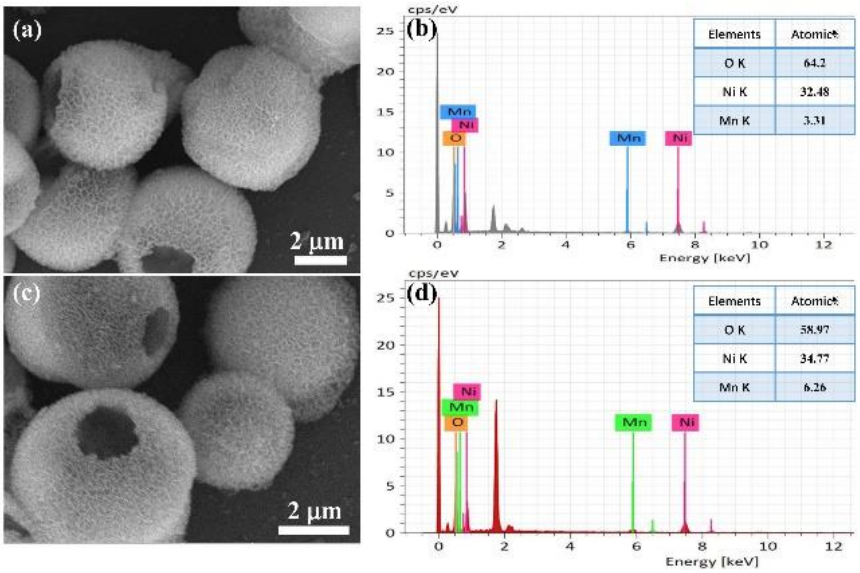

Fig. S8 (a) FESEM image of α-$Ni(OH)_2/Mn_2O_3$ microspheres with $KMnO_4$ treatment for 5 min and (b) corresponding EDS spectrum. (c) FESEM image of α-$Ni(OH)_2/Mn_2O_3$ with $KMnO_4$ treatment for 30 min and (d) corresponding EDS spectrum.

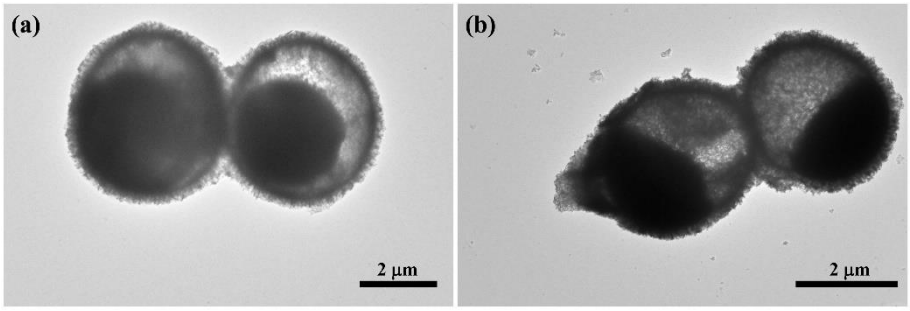

Fig. S9 TEM images of α-$Ni(OH)_2/Mn_2O_3$ with $KMnO_4$ treatment for 5 min (a) and 30 min (b), respectively.

In order to study the effects of the time of $KMnO_4$ treatment on the performances of the $Ni(OH)_2/Mn_2O_3$ microspheres. Two control $Ni(OH)_2/Mn_2O_3$ microsphere samples with $KMnO_4$ treatment have been synthesized by the same methods except for the time of $KMnO_4$ treatment. The morphological structure of the as-synthesized control $Ni(OH)_2/Mn_2O_3$ microspheres has been investigated by FESEM and TEM, their supercapacitive properties have been studied using CV and GCD measurements.

As shown in Fig. S8 and S9, when treated with $KMnO_4$ solution for 5 min or 30 min, the microspheres all retain their yolk-shell microstructures decorated by plentiful and interconnected nanosheets. The corresponding EDS spectrum show that the Mn content on the microsphere surface increases with the time of $KMnO_4$ treatment. When treated for 5 min, there is only about 3.31 at.% of Mn in the composite (Fig. S8b), which is lower than that of the microspheres treated for 15 min (4.56 at.%, Fig. S3). With the prolongation of the treatment to 30 min, Mn content in the composite increases to about 6.26 at.% (Fig. S8d), meanwhile the corresponding microspheres exhibit relatively denser coating due to the more Mn_2O_3 deposition (Fig. S9b).

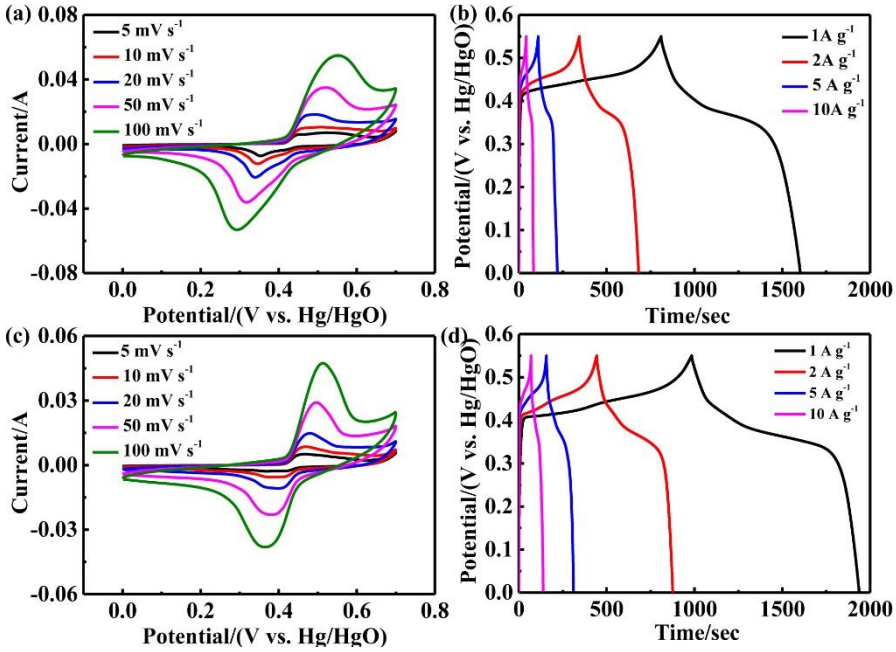

Fig. S10 Capacitance performance of as-synthesized microspheres in 1 M KOH: (a) CV curves and (b) GCD curves of the α-$Ni(OH)_2/Mn_2O_3$ microspheres with $KMnO_4$ treatment for 5 min at various scanning rates, (c) CV curves and (d) GCD curves of the α-$Ni(OH)_2/Mn_2O_3$ microspheres with $KMnO_4$ treatment for 30 min at various scanning rates.

The CV tests of the as-prepared control microspheres are performed at the sweep rate of 5 mV s^{-1} to 100 mV s^{-1} in the voltage window range from 0.0 V to 0.7 V (vs. Hg/HgO) (Fig. S10a, c). The curves all exhibit obvious redox peaks, symbolizing the representative pseudocapacitive behavior, which could be attributed to the Ni^{+2}/Ni^{+3} redox conversion. The cathodic and anodic peaks shift as scanning rate increasing because of the polarization influence on the electrode. The GCD curves show that the α-$Ni(OH)_2/Mn_2O_3$ microspheres treated with $KMnO_4$ for 5 min display the specific capacitances of 1442, 1228, 988 and 744 F g^{-1} at 1, 2, 5 and 10 A g^{-1}, respectively (Fig. S10b). While the α-$Ni(OH)_2/Mn_2O_3$ microspheres treated with $KMnO_4$ for 30 min possess relatively higher specific capacitances of 1733, 1574, 1405 and 1253 F g^{-1} at 1, 2, 5 and 10 A g^{-1}, respectively (Fig. S10d). However, the specific capacitances of both control samples are significantly lower than those of the $Ni(OH)_2/Mn_2O_3$ microspheres treated with $KMnO_4$ for 15 min (Fig. 7b).

From the above experimental results, we believe that the appropriate Mn_2O_3 sediment on the α-$Ni(OH)_2/Mn_2O_3$ microspheres could enable high reversible capacitance via a created faster electron conduction path. Too little Mn_2O_3 sediment can't create effective electron conduction path for enhanced capacitance, while too thick Mn_2O_3 sediment may slow down the reactant or charge transfer around the microspheres during their electrochemical reaction process. Therefore, it appears that the $Ni(OH)_2/Mn_2O_3$ microspheres could achieve the optimum electrochemical performance with $KMnO_4$ treatment for 15 min (4.5 at.% of Mn), at this point these opposing factors reach an ideal compromise.

Table S2 Comparison of the electrochemical performances for α-$Ni(OH)_2/Mn_2O_3$ yolk-shell hierarchical microspheres with the reported Ni- and Mn-based electrodes.

Active material	**Specific capacitance (F g^{-1})**	**Capacitance retention**	**Ref.**
Hierarchical $Ni(OH)_2$-MnO_2@C/NF	1608.5 (at 0.67 A g^{-1})	93.9% (10 A g^{-1} after 5000 cycles)	[3]
Sponge-like NiMn@Mn	2093 (at 1 A g^{-1})	62% (5 A g^{-1} after 10,000 cycles)	[4]
Ultrathin $Ni(OH)_2$ nanosheets	2384.3 (at 1 A g^{-1})	75% (5 A g^{-1} after 3000 cycles)	[5]
Ultrathin sheet-like Ni/Co hydroxides	2654.9 (at 1 A g^{-1})	77% (10 A g^{-1} after 1500 cycles)	[6]
Core-shell $NiCo_2O_4/MnO_2$	1471.4 (at 10 mA cm^{-2})	88% (10 mA cm^{-2} after 2000 cycles)	[7]
$Ni(OH)_2$-MnO_2/rGO	1985 (at 2 A g^{-1})	75% (8 A g^{-1} after 2000 cycles)	[8]
Core-shell $Ni(OH)_2$@Mn_2O_3	1219.1 (at 2 A g^{-1})	90% (2 A g^{-1} after 1000 cycles)	[9]
$Ni(OH)_2/Mn_2O_3$ yolk-shell microspheres	2228.6 (at 1 A g^{-1})	77.7% (10 A g^{-1} after 3000 cycles)	This work

Resulting from the distinctive synergistic effect of the yolk-shell microstructure and hetero-composition characteristics, the α-$Ni(OH)_2/Mn_2O_3$ microspheres display an outstanding high specific capacitance (2228.6 F g^{-1} at 1 A g^{-1}) and a competitive cycling stability (capacitance retention of 77.7% after 3000 cycles at 10 A g^{-1}). Which appears quite attractive even if compared with the other Ni- and Mn-based electrodes for high-performance supercapacitor as summed up in Table S2.

References

1. Zhao W, Zhou X, Kim I J, Kim S. Self-assembled Co_3O_4 hexagonal plates by solvent engineering and their dramatically enhanced electrochemical performance. Nanoscale, 2016, 9(2): 940-946

2. Wang D W, Guan B, Li Y, Li D D, Xu Z Y, Hu Y F, Wang Y Q, Zhang H H. Morphology-controlled synthesis of hierarchical mesoporous α-$Ni(OH)_2$ microspheres for high-performance asymmetric supercapacitors. Journal of Alloys and Compounds, 2017, 737: 238-247

3. Li J B, Cao W, Zhou N, Xu F, Chen N, Liu Y, Du G P. Hierarchically nanostructured $Ni(OH)_2$-MnO_2@C ternary composites derived from Ni-MOFs grown on nickel foam as high-performance integrated electrodes for hybrid supercapacitors. Electrochimica Acta, 2020, 343: 136139-136149

4. Feng L Y, Sun J K, Liu Y H, Li X X, Ye L, Zhao L J. 3D sponge-like porous structure of Mn_2O_3 tiny nanosheets coated on $Ni(OH)_2$/Mn_2O_3 nanosheet arrays for quasi-solid-state asymmetric supercapacitors with high performance. Chemical Engineering Journal, 2018, 339: 61-70

5. Xiong X H, Ding D, Chen D C, Waller G, Bu Y F, Wang Z X, Liu M L. Three-dimensional ultrathin $Ni(OH)_2$ nanosheets grown on nickel foam for high-performance supercapacitors. Nano Energy, 2015, 11: 154-161

6. Ye L, Zhao L J, Zhang H, Zhang B, Wang H Y. One-pot formation of ultra-thin Ni/Co hydroxides with a sheet-like structure for enhanced asymmetric supercapacitors. Journal of Materials Chemistry A, 2016, 4: 9160-9168

7. Yu L, Zhang G Q, Yuan C Z, Lou X W. Hierarchical $NiCo_2O_4$@MnO_2 core-shell heterostructured nanowire arrays on Ni foam as high-performance supercapacitor electrodes. Chemical Communications, 2013, 49(2): 137-139

8. Chen H, Zhou S X, Wu L M, Porous nickel hydroxide-manganese dioxide-reduced graphene oxide ternary hybrid spheres as excellent supercapacitor electrode materials. ACS Applied Materials Interfaces, 2014, 6(11): 8621-8630

9. Ren Q, Wang R F, Wang H, Key J L, Brett D J L, Ji S, Yin S B, Shen P K. Ranunculus flower-like $Ni(OH)_2$@Mn_2O_3 as a high specific capacitance cathode material for alkaline supercapacitors. Journal of Materials Chemistry A, 2016, 4(20): 7591-7595